www.rericjournal.ait.ac.th

CFD based Analysis of a Solar Air Heater having Isosceles Right Triangle Rib Roughness on the Absorber Plate

Rajeev Ranjan*[1], M.K. Paswan* and N. Prasad*

Abstract – *In the present work the study of heat transfer and friction characteristics in rectangular duct of a solar air heater having isosceles right triangle rib shape on the absorber plate by using CFD (Computational Fluid Dynamics) The roughness has been placed in such way that the hypotenuse faces against the flow direction. The design parameters chosen for study are Reynolds number, roughness height and roughness pitch. The turbulence model used in CFD solutions is Renormalization group (RNG) k-ε. The roughness height (e) is chosen as 0.5mm, 1.0mm and 1.5mm at roughness pitch (P) of 5mm, 10mm, 15mm and 20mm. The relative roughness Pitch (P/e=3.33-40) and relative roughness height (e/D= 0.015-0.045) is taken. The effect of transverse wedge shape on heat transfer and friction factor was investigate covering the range of roughness parameter having Reynolds no varies from 3000 to 18000. ANSYS FLUENT is used to simulate turbulent airflow in artificial roughened solar air heater. Five different turbulence models is tested on the quality of obtained results .The RNG k-ε model yield better result for two dimensional flow through conventional solar air heaters. Thermo-hydraulic performance is also calculated. Correlations for the Nusselt number and friction factor have been developed.*

Keywords – Artificial roughness, CFD, heat transfer, solar air heater, thermo-hydraulic performance.

1. INTRODUCTION

Solar energy is the most abundant, pollution free and inexhaustible form of energy available on earth. The solar air heater can be used as a sub-system in many applications meant for the utilization of solar energy such as drying or curing of agricultural products, space or room heating for comfort, regeneration of dehumidifying agents, seasoning of timber, curing of industrial products such as plastics. Their usefulness as also the quantitative energy collection has been limited because of lower thermal efficiency primarily as a result of lower convective heat transfer coefficient between the absorber plate and air leading to higher plate temperature and greater thermal losses.

A number of investigations have been carried out on the heat transfer characteristics of channel or pipes with roughness elements on the surface. The concept of artificial roughness was first applied by Joule [1] to enhance heat transfer coefficients for in-tube condensation of steam and since then many experimental investigations were carried out on the application of artificial roughness in the areas of cooling of gas turbine, electronic equipment, nuclear reactors, and compact heat exchangers *etc*. Nunner [2] was the first who developed a flow model and likened this model to the temperature profile in smooth tube flow at increased Prandtl number. The proposed flow model predicts that roughness reduces the thermal resistance of the turbulence dominated wall region without significantly affecting the viscous region. A friction correlation for flow over sand-grain roughness was developed by Nikuradse [3]. Based on law of the wall similarity, Nikuradse presented the pressure drop results in terms of roughness function R and roughness Reynolds number e+. Dipprey and Sabersky [4] developed a heat-momentum transfer analogy relation for flow in a sand-grain roughened tube and achieved excellent correlation of their data. The concept proposed by Dipprey and Sabersky was so common and it can be applied to any roughness for which law of the wall similarity holds. Prasad and Mullick [5] were the first who introduced the application of artificial roughness in the form of small diameter wire attached on the underside of absorber plate to improve the thermal performance of solar air heater for drying purposes. After Prasad and Mullick's [5] work, a number of experimental investigations on solar air heater involving roughness elements of different shapes, sizes and orientations with respect to flow direction have been carried out in order to obtain an optimum arrangement of the roughness element geometry by Hans VS, Saini RP, Saini JS [6]; Bhushan B, Singh R [7]; Kumar A, Saini RP, Saini JS [8]. Karwa *et al.* [9] conducted an experimental investigation of the performance of solar air heaters with chamfered repeated rib-roughness on the air flow side of the absorber plates. The authors found substantial enhancement in thermal efficiency (10-40%) over solar air heaters with smooth absorber plates. Saini and Verma [10] conducted an experimental investigation on fluid flow and heat transfer characteristics of solar air heater duct having dimple-shaped artificial roughness. The authors found the maximum value of Nusselt number corresponds to the relative roughness height (e/D) of 0.0379 and relative roughness pitch (P/e) of 10. The authors also found minimum value of friction factor correspond to the relative roughness height (e/D) of 0.0289 and relative pitch (P/e) of 10. Singh *et al.* [11] experimentally investigated the heat transfer characteristics of rectangular duct having its one broad

*Mechanical Engineering Department, National Institute of Technology Jamshedpur, Jamshedpur-831014, India.

[1]Corresponding author;
Tel: +919798715609.
E-mail: rajeev3278@yahoo.co.in.

wall heated and roughened with periodic 'discrete V-down rib'. The authors found the maximum value of Nusselt number and friction factor corresponds to relative roughness pitch (P/e) of 8. Tanda [12] experimentally investigated the heat transfer coefficients and friction factors for a rectangular channel having one wall roughened having angled continuous ribs, transverse continuous and broken ribs, and discrete V-shaped ribs. Author reported that roughening the heat transfer surface by transverse broken ribs appeared to be the most promising enhancement technique for investigating rib geometries. Lanjewar *et al.* [13] carried out an experimental investigation on heat transfer and friction factor characteristics of rectangular duct roughened with W-shaped ribs. Author reported that thermo-hydraulic performance improved with angle of attack of flow and relative roughness height and maxima occurred at angle of attack 60°. Bhagoria *et al.* [14] performed experiments to determine the effect of relative roughness pitch, relative roughness height and wedge angle on the heat transfer and friction factor in a solar air heater roughened duct having wedge shaped rib roughness. Authors found maximum enhancement of Nusselt number up to 2.4 times while the friction factor up to 5.3 times for the range of parameters investigated. Kumar *et al.* [15] experimentally investigated heat transfer and friction characteristics in solar air heater by using discrete W-shaped roughness on one broad wall of solar air heater. The maximum enhancement of Nusselt number and friction factor as a result of providing artificial roughness was found to be 2.16 and 2.75 times than that of smooth duct for an angle of attack 60° and relative roughness height of 0.0338. Yadav and Bhagoria [16] conducted CFD investigations of an artificially roughened solar air heater to examine the effect of circular transverse ribs roughness on the absorber plate. 2D CFD simulation of the duct was based on CFD code FLUENT v12.1. The simulation results revealed that RNG k -ε turbulence models predicted flow distribution and heat transfer very well. A CFD simulation was conducted with different turbulence models in order to find out the best appropriate turbulence model for simulation of artificially roughened solar air heater. The results obtained by the RNG k − ε model were in good agreement with the Dittus–Boelter and Blasius empirical correlations. Yadav and Bhagoria [17] conducted a numerical analysis of the heat transfer and flow friction characteristics in an artificially roughened solar air heater having square sectioned transverse rib roughness considered at the underside of the top heated wall. The thermohydraulic performance parameter under the same pumping power constraint was calculated in order to examine the overall effect of the relative roughness pitch. The maximum value of the thermohydraulic performance parameter was found to be 1.82 corresponding to a relative roughness pitch of 10.71. Chaube *et al.* [18] used FLUENT 6.1 CFD Code and SST k-ε as a turbulence model for analysis of ten different types of ribs, namely rectangular, square, chamfered, triangular and so forth. FLUENT 6.3.26 Code and renormalization group (RNG) k-ε turbulence model was used by Kumar and Saini [19] to simulate artificial roughness. Karmare and Tikekar [20] have carried out simulation of fluid flow and heat transfer in a solar air heater duct with metal grit as a roughness element of circular, square and triangular cross section, having an angle of attack 54°, 56°, 58°, 60° and 62°, were tested on small Reynolds number. Hans *et al.* [21] study on heat transfer and friction factor for a solar air heater with multiple v-ribs. A maximum enhancement of Nusselt number and friction factor due to presence of such an artificial roughness has been found to be 6 and 5 times, respectively, in comparison to the smooth duct for the range of parameters. Correlations for Nusselt number and friction factor in terms of roughness geometry and flow parameters were developed.

Conventional technique used for designing an artificial roughened solar air heater is most tedious, expensive and time taking. CFD approach is a cost effective alternative and less time taking. The solution obtained from CFD simulations is largely within the acceptable range. CFD is an effective tool for predicting the behavior and performance of an artificial roughened solar air heater. Apart from this, many researchers have carried out

In the present work a CFD analysis of transverse rib roughness with isosceles with right triangle cross-section is conducted. The upper wall is subjected to uniform flux condition while the lower wall is insulated. The ribs are provided underside of the absorber plate and side are kept smooth. The main objective of the present work is to study the effect of relative roughness pitch (P/e) and Reynolds number (Re) on Nusselt number and friction factor, flow parameters and roughness parameter on flow fields, and temperature field and heat transfer and also find optimal roughness geometry for maximum thermo-hydraulic performance. Correlations for the nusselt number and friction factor have been also developed

2. NUMERICAL MODEL AND SOLUTION PROBLEM

Step 1: Select system and operating Parameters. In this case CFD analysis and creation of the geometry of the flow region, *i.e* the computational domain for CFD calculation.

Step 2: In the second step mesh generation is done after the definition of the domain geometry. CFD requires the sub-division of the domain into a number of small, non-overlapping sub domains in order to solve the flow physics within the domain geometry that has been created this results in the generation of mesh (or grid) of cells (elements or control volume) overlying the whole geometry. The essential fluid flow that are described in each of these cells are usually solved numerically, so that the discrete values of the flow properties, such as velocity, temperature, pressure, and other transport parameters of interest, are determined.

Step 3: Selection of Physics and Fluid Properties.

Step 4: Select a Boundary condition for the mathematical model. The boundary condition consist inlet, outlet, top surface, bottom surface of isosceles right triangle.

Step 5: Now CFD solver posses two step *i.e* initialization and solution control. Before initialization of problem iterative procedure generally requires all the discrete value of the flow properties, such as the velocity, pressure, temperature and other transport parameters should be resolved. Here second-order upwind scheme is selected for energy and momentum equation.

Step 6: In this step CFD solver operate three process *i.e.* monitoring solution, CFD calculation and checking for convergence. The SIMPLE algorithm (semi-implicit method for pressure and velocity). The convergence criteria of 10^{-3} for the residuals of the continuity equation 10^{-6} for the velocity components and 10^{-6} for the residuals of the energy.

Step 7: The Re is calculated from

$$Re = \rho u D/\mu$$

Step 8: The Nusselt number is calculated for roughened duct

$Nu_r = \frac{hD}{k}$ Where h is average convective heat transfer co-efficient and calculated from CFD

Step 9: The friction factor is calculated by pressure drop, ΔP across the length of the test section and obtained by

$$fr = \frac{(\Delta P/l)D}{2\rho V^2}$$

Step 10: For Smooth duct Blasius equation is taken for friction factor

$$F_s = 0.0791\ Re^{-0.025}$$

CFD simulation of two-dimensional artificially roughened solar air heater duct along transverse ribs roughness with isosceles right triangle cross-section as a vortex generator in inlet section is carried out using the CFD software package ANSYS FLUENT (version 14.5). The general assumption, consider in the analysis are as follows:

1. The flow is steady, two dimensional, turbulent and fully developed.
2. The flow is single phase across the duct.
3. The walls in contact with fluid are assigned, no-slip boundary condition.
4. The duct wall, absorber plate and roughness material are homogeneous and isotropic. The thermodynamic properties of air and the absorber plate (aluminum) are considered constant.
5. The effect of radiation heat transfer and other heat losses are considered less.

2.1. Computational Solution Domain

In the present numerical study of artificial roughened solar air heater having isosceles right triangle rib roughness is simulated. In the analysis two dimensional (2-D) computational domain is adopted because 2-D flow model yield the results closer measurements as compared to that with 3-D flow Chaube *et al.* [18]. Therefore 2-D flow is carried out for saving computer memory and computational time. The domain consist three sections *i.e* an entry section [L1], a test section [L2] and exit section [L3] as per ASHRAE standard (93-2003) [22]. A short entrance length is selected because for a roughened duct, the thermally fully developed is established is a short length of 2 to 3 times of hydraulic diameter. The exit section is used after the test section in order to reduce the end effect in the test section.

The geometric model developed for the current study is as shown in Figure 1.

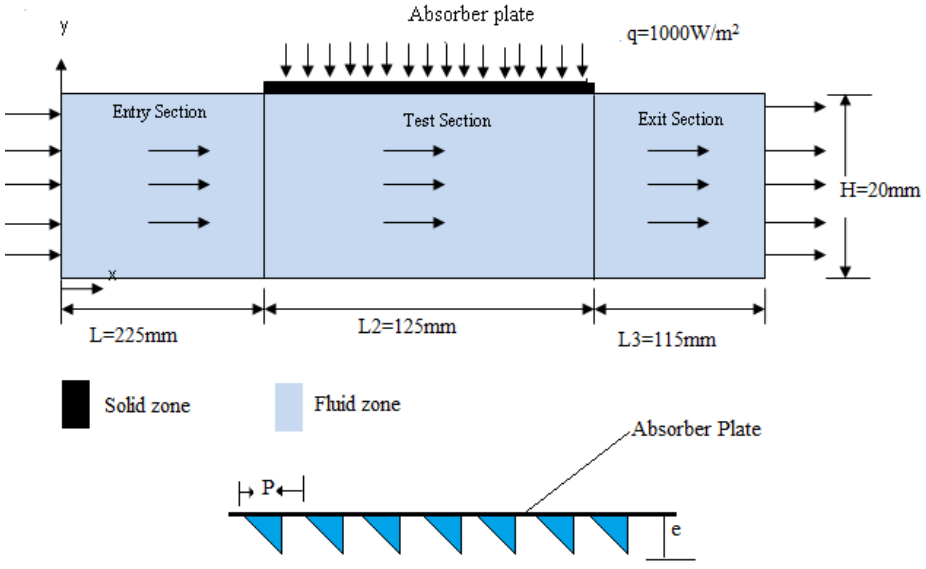

Fig. 1. Computational domain.

The modeling software used here is ANSYS Design Modeler v 14.5.The model was created as a surface geometry. The geometry consists of three sections, namely entry section, test section and exit section which are 225mm, 125mm and 115mm long respectively. The duct height is 20mm and an absorber plate of 0.5mm thickness is placed above the test section. The entry section is provided so that the flow becomes fully developed before it enters the test section. The exit section is provided to avoid the end effect from travelling upstream into the test section (as the flow is sub-sonic). According to ASHRAE standards 93-2003, an entrance and exit length of $5\sqrt{WH}$ and $2.5\sqrt{WH}$ respectively are provided [22].

2.2. Boundary Conditions

The boundary condition for different edges has been created while constructing the geometry of grid in ANSYS ICEM CFD v 14.5. The inlet is given as velocity-inlet boundary condition. The outlet is given as pressure-an outlet boundary condition with pressure being equal to atmospheric pressure $1.013X10^5$ pa is applied at the exit. The top-surface of the study domain is given as a constant heat flux *i.e* $1000W/m^2$ boundary condition with heat flux being equal to solar insolation. The bottom wall kept at adiabatic wall condition. The working fluid in all cases is taken as air and absorber plate material is taken as aluminum. The inside air temperature of the duct is 300K is taken. No-slip boundary condition is given along the wall. The turbulence intensity at the core of fully developed flow is calculated using the empirical correlation given below:

$$I = 0.16\ Re^{-1/8} \quad (1)$$

The material properties are shown in Table 1. The range of geometrical and operating parameters employed in this computational investigation is shown in Table 2.

Table 1. Properties of the materials used in the computational domain.

Properties	Air	Aluminum
Density, 'ρ' (kg/m^3)	1.225	2719
Specific Heat, 'C_p'(J/kg-K)	1006.43	871
Thermal Conductivity 'k' (W/m-K)	0.0242	202.4
Viscosity,'μ' (N/m^2)	$1.7894x10^{-5}$	-

Table 2. Geometrical and operating parameters.

Geometrical and Operating Range	Parameters
Entry length,L1	225mm
Test Section length,L2	125mm
Exit length,L3	115mm
Width of duct, W	100mm
Depth of duct, H	20mm
Hydraulic diameter of duct, D	33.33mm
Duct aspect ratio, W/H	5
Uniform flux, 'q'	$1000W/m^2$
Reynolds number, Re	3593-15000(6 values)
Rib height, e	0.5, 1, 1.5
Rib Pitch,P	5, 10, 15, 20
Relative Roughness pitch, 'P/e'	3.33-40 (12 values)
Relative Roughness height,(e/D)	0.015-0.045(3 values)
Prandtl number, 'Pr'	0.7441

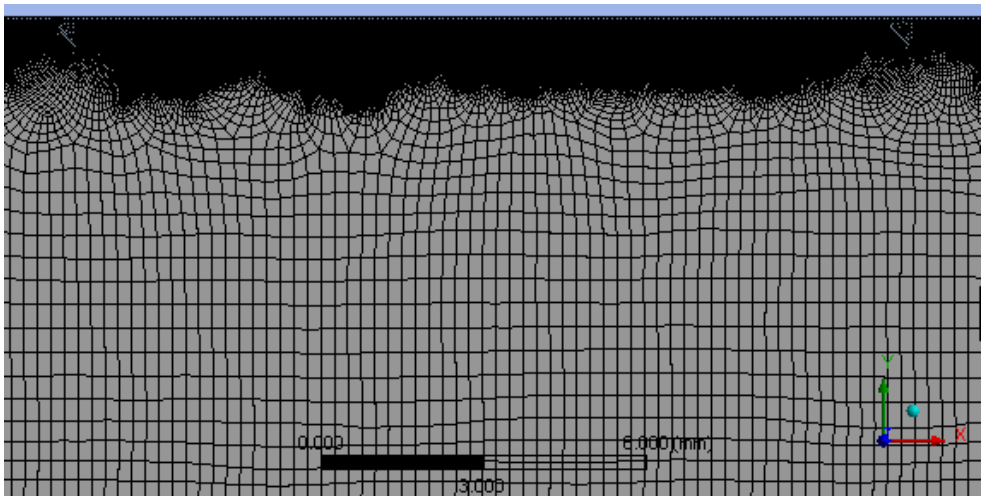

Fig. 2. Mesh geometry.

2.3. Geometry Meshing

The meshing software used here is ANSYS ICEM CFD V 14.5. The non-uniform grids are generated for all numerical simulations performed in this CFD work. To obtain better results the entire fluid flow zone is sub-divided into many zones and a combination of structured (mapped) and unstructured mesh was created in the fluid domain. The fluid flow zone near the roughness element was further refined to reduce the cell size to 0.025mm in order to resolve the laminar sub-layer. The meshed geometry with quad element, generated for 5mm pitch and 0.5mm roughness height geometry having 221730 numbers of cells is as shown in Figure 2. A grid independence test is implemented over grids with different numbers of cells. It is found that the variation in Nusselt number and friction factor marginally increases when moving from 211,226 cells to 236,886. Hence, there is no such advantage in increasing number of cells beyond this value. Thus, the grid system of 211,226 cells is adopted for the current computation.

2.4. Governing Equations and Data Reduction

The flow field in this problem is governed by steady state, two dimensional, incompressible hence continuity, conservation of momentum, and energy equations are used to solve the forced turbulent fluid flow and heat transfer in the artificially roughened solar air duct. The governing equations in the rectangular cartesian coordinate system can be written as follows:-

Continuity equation:

$$\frac{\partial}{\partial x_i}(\rho u_i) = 0 \tag{2}$$

Momentum equation:

$$\frac{\partial}{\partial x_i}(\rho u_i u_j) = -\frac{\partial p}{\partial x_i} + \frac{\partial}{\partial x_j}\left[\mu\left(\frac{\partial u_i}{\partial x_j} + \frac{\partial u_j}{\partial x_i}\right)\right] + \frac{\partial}{\partial x_j}\left(-\rho\overline{u_i' u_j'}\right) \tag{3}$$

Energy equation:

$$\frac{\partial}{\partial x_i}(\rho u_j T) = \frac{\partial}{\partial x_j}\left((\Gamma + \Gamma_t)\frac{\partial T}{\partial x_j}\right) \tag{4}$$

Where Γ and Γ_t are molecular thermal diffusivity and turbulent thermal diffusivity respectively.

$$\Gamma = \frac{\mu}{Pr} \text{ and } \Gamma_t = \frac{\mu_t}{Pr_t}$$

Equations 2 and 4 are called Reynolds Averaged Navier-Stokes equation (RANS). The additional term $-\rho\overline{u_i' u_j'}$ in Equation 3 is called Reynolds stress and is responsible for capturing the effects of turbulence. But this additional term requires us to add two more equations in order to get a closed form of equation. A common way is to use Boussinesq Hypothesis to relate the Reynolds stress to mean velocity gradient as given below:

$$-\rho\overline{u_i' u_j'} = \mu_t\left(\frac{\partial u_i}{\partial x_j} + \frac{\partial u_j}{\partial x_i}\right) \tag{5}$$

The Boussinesq hypothesis is implemented here using RNG k-epsilon turbulence model:

$$\frac{\partial}{\partial x_i}(\rho k u_i) = \frac{\partial}{\partial x_j}\left(\alpha_k \mu_{eff}\frac{\partial k}{\partial x_j}\right) + G_k - \rho\varepsilon \tag{6}$$

$$\frac{\partial}{\partial x_i}(\rho \varepsilon u_i) = \frac{\partial}{\partial x_j}\left[\alpha_\varepsilon \mu_{eff}\frac{\partial \varepsilon}{\partial x_j}\right] + C_{1\varepsilon}G_k\frac{\varepsilon}{k} - C_{2\varepsilon}\rho\frac{\varepsilon^2}{k} - R_\varepsilon \tag{7}$$

Where μ_{eff} is the effective turbulent viscosity and μ_t is the turbulent viscosity and is given by

$$\mu_{eff} = \mu + \mu_t \tag{8}$$

$$\mu_t = \rho C_\mu \frac{k^2}{\varepsilon} \tag{9}$$

In Equations 6 and 7, G_k represents the generation of turbulence kinetic energy due to the mean velocity gradients and is given by:

$$G_k = -\rho\overline{u_i' u_j'}\frac{\partial u_j}{\partial x_i} \tag{10}$$

$C_{1\varepsilon}$, $C_{2\varepsilon}$, C_μ, α_k and α_ε are constants and their respective default values are: $C_{1\varepsilon}$=1.42, $C_{2\varepsilon}$=1.68, C_μ=0.0845, α_k=1.39 and α_ε=1.39.[23]

Different model namely Renormalization group (RNG) K-ε model, standard k-ε model, standard k-ε model, standard k- model, shear stress transport k- have been tested for smooth duct having same cross section of roughened duct in order to find out the validity of cross-section of roughened duct in order to find out the validity of the models .The results obtained by different models have been compared with Dittus-Boelter empirical correlation for Nusselt number given below for smooth duct.

$$Nu_s = 0.023 Re^{0.8} Pr^{0.4} \tag{11}$$

Figure 3 shows the variation of Nusselt number with Reynolds number using for different models and results are compared with Dittus-Boelter empirical correlation for smooth duct of a solar air heater. It has been observed that the results obtained by Renormalization–group (RNG) k-ε models are in good agreement with Dittus-Boelter empirical correlation results. It is therefore, for the present numerical study Renormalization-group (RNG) k-ε model has been employed to simulate the flow and heat transfer.

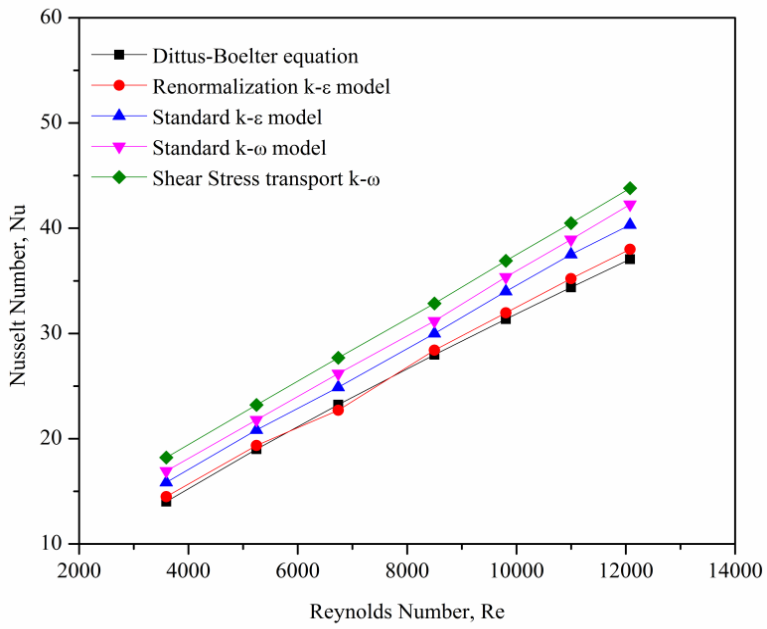

Fig. 3. Comparison between Nusselt numberpredictions of different CFD models with Dittus-Boelter empirical relationship for smooth duct.

The use of the transverse ribs with isosceles right triangle results enhancement in heat transfer, which is predicted by calculating average Number for the roughened solar air heater. This enhancement is also accompanied by an increase in friction factor. The friction is calculated from pressure drop, $^{\Delta}$P across the cross- section of artificial roughened solar air heater.
The average Nusselt number for artificially roughened solar air heater is computed as

$$Nu = \frac{h.D}{k} \tag{12}$$

Where *h* is the average heat transfer coefficient.

The average friction factor for artificially roughened solar air heater

$$f = \frac{\Delta p.D}{2\rho l v^2} \tag{13}$$

The performance of solar air heater using artificial roughness results enhancement of air heater and enhancement of friction losses. So it is desirable that design of artificial roughness should be in such a way that it breaks the sub-layer thickness without disturbing the already existing turbulent core to keep the pressure at a low level, increasing the heat transfer coefficient between the absorber plate and the flowing air over it and thereby increasing the heat transfer while reducing the heat losses. Inclusion of artificial roughness results additional frictional factor which leads to more pumping power.

For the optimum performance, we should consider both the thermal effect, *i.e.* the enhancement in heat transfer rate and also the hydraulic effect *i.e.* the increase in pressure drop across the duct. To consider both these effects together the thermo-hydraulic performance is calculated. An alternate form of this equation using Stanton number was first proposed by Webb and Eckert [24]. It is defined as:

$$\eta_{THPP} = \frac{Nu_r/Nu_s}{\left(f_r/f_s\right)^{1/3}} \tag{14}$$

Where Nu is the Nusselt number and f is the friction factor. The subscript r and s signify rough and smooth absorber plate.

The friction factor and the Nusselt number for the smooth absorber plate where taken from the semi-empirical relations. The friction factor was calculated from Blasius equation [26].

$$f_s = 0.0791\ Re^{-0.25} \tag{15}$$

The Nusselt number for the smooth absorber plate was calculated from Dittus-Boelter equation [25].

$$Nu_s = 0.023\ Re^{0.8} Pr^{0.4} \tag{16}$$

2.5 Validation

The friction factor and Nusselt number determined from CFD data for smooth duct have been compared with the values obtained from Blasius (Equation 26) and Dittus-Boelter (Equation 25), respectively. The average percentage deviation of the CFD data of friction factor and Nusselt number from the values predicted by correlation has been found to ±8.5% and ±9%. Figure 4 and Figure 5 show the comparison of CFD data and predicted values of friction factor and Nusselt number respectively. This shows good agreement between CFD data obtained from present work and a predicted value establishes the accuracy of the value taken from CFD analysis.

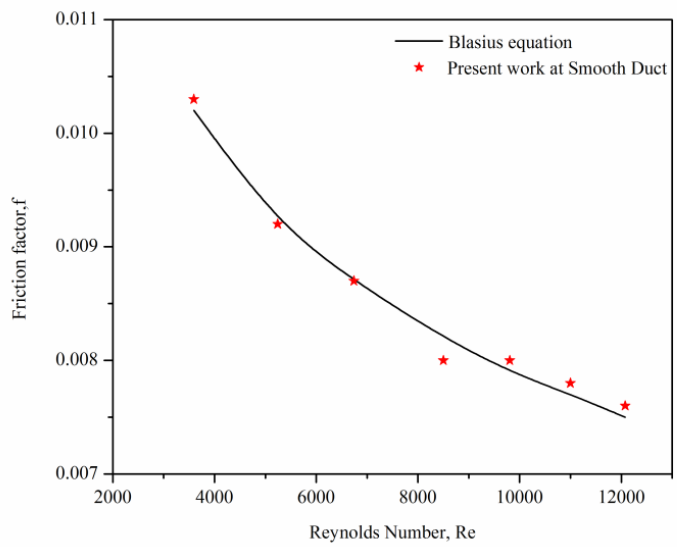

Fig. 4.Variation of friction factor present work and Blasius equation for smooth duct.

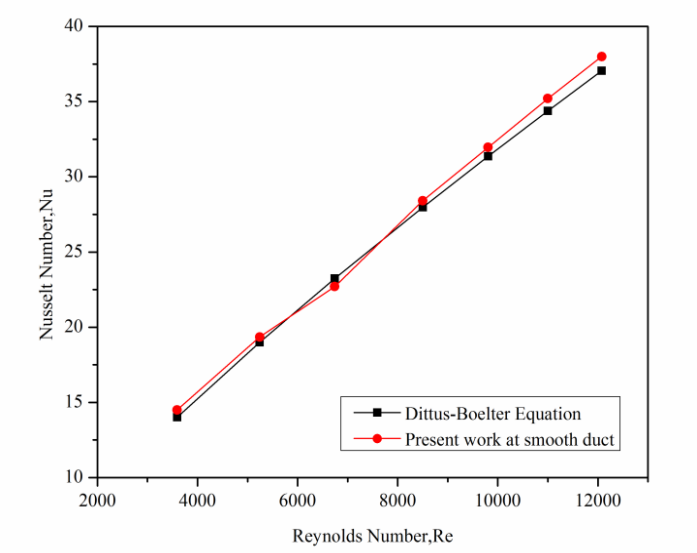

Fig. 5. Comparison of Nusselt number present work and Dittus-Boelter equation for smooth duct.

3. RESULTS AND DISCUSSION

The effects of various fluid flow parameters and roughness geometry parameters on the heat transfer and friction characteristics of the flow of air on a roughened absorber plate are presented below. The results have been compared with those obtained in case of smooth absorber plate operating under similar conditions to discuss the enhancement of heat transfer and friction factor due to the introduction of artificial roughness.

3.1 Flow and Temperature Fields

Contour plots for velocity magnitude at different rib height at pitch P=5 and Reynolds number= 5000 is shown in Figures 5 to 7. It is observed that turbulence created by the ribs increases turbulence kinetic energy and turbulence dissipation rate, which in turn breaks the laminar sub layer thickness and increases the heat transfer coefficient. It further reduces thermal resistance in the direction of flow result in increasing in Nusslet number. By increasing velocity with increasing value of Reynolds number, which results in enhanced heat transfer rate.

Figures 8 to 10 show us the contour plots for static temperature at different Reynolds number. It can be seen that as the Reynolds number increases the static temperature of the flow field decreases. It can also be observed that the diffusion of temperature into the core of the flow field decreases as the Reynolds number increases, but the near wall diffusion of temperature increases as the Reynolds number increases. Figures 11 to 13 show us the contour plots for turbulence intensity at different Reynolds number. It can be seen that the peak value of the turbulent intensity is found on the top of rib front region and it decreases with an increase in the distance from the wall. This can be attributed to the formation of eddies in the vicinity of the wall due to the high shear stress which defuses in the main flow. Figure 14 shows variation of friction factor vs. Reynolds number at different P/e and fixed e/D *i.e* 0.03. It is seen from figures that the friction factor decreased monotously with increase it Reynolds number. Presence

of isosceles right triangle sectional rib causes an additional loss of energy resulting in increase in average friction factor than smooth. It can also see that average friction factor decreases with the increase in Reynolds number because of the suppression in laminar sub layer due to presence of rib which cause high pressure drop no significant increase in heat transfer. Figure 15 shows the variation of Nusselt number with the Reynolds number for different values of relative roughness pitch (P/e) and for fixed value of relative roughness height (e/D). It has been observed that Nusselt number increases with an increase in Reynolds number. This is due to the presence of isosceles right triangle rib roughness on the absorber plate lead to superior heat transfer performance on the secondary flow induced by the top rib. Secondary flow has two counter-rotating vortices, carry cold fluid from the central core region toward the rib wall. This secondary flow interaction with main flow, affect the flow reattachment and recirculation between transverse ribs.

Figure 16 shows variation of friction factor versus relative roughness pitch at fixed e/D=0.03. It shows that at fixed relative roughness height friction factor decreases with an increase of relative roughness Pitch and decreases with increasing values of the Reynolds number. Figure 17 show variation of Nusselt number vs. Relative roughness pitch, P/e at fixed e/D=0.03. It is found that Nusselt number decreases with an increase of relative roughness pitch and increases with increasing value of Reynolds number in all cases.

Isosceles right triangle rib with relative roughness height of 0.045 provides the highest friction factor.

Figure 18 shows the variation of friction factor as a function of relative roughness height for P/e=10.It has been found that at fixed relative roughness pitch the friction factor increases with an increase of relative roughness height. Figure 19 shows Nusselt number as a function of relative roughness height for P/e=10.It has been found that Nusselt number increases with an increase of relative roughness height. Figure 20 shows variation of friction factor with Reynolds number and for different values of e/D and fixed value of P/e. It has been found friction factor decreases with the increase in Reynolds number for different value of relative roughness height (e/D). Figure 21 shows variation of Nusselt number with Reynolds number and for different values of e/D and fixed value of P/e..It has been seen that Nusselt number increases with increasing Reynolds number at different values of relative roughness height (e/D).

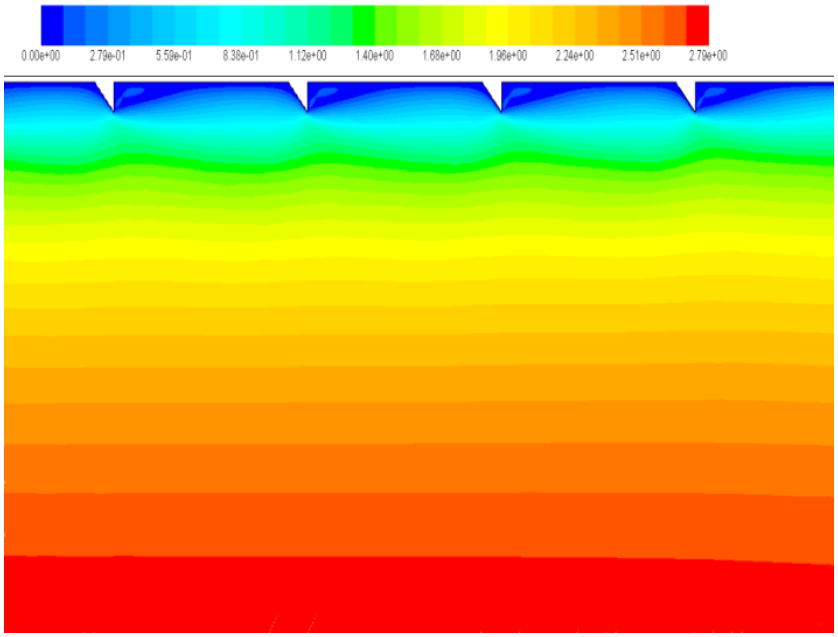

Fig. 6. Contour Plot for velocity magnitude for e=0.5 P=5 Re=5000.

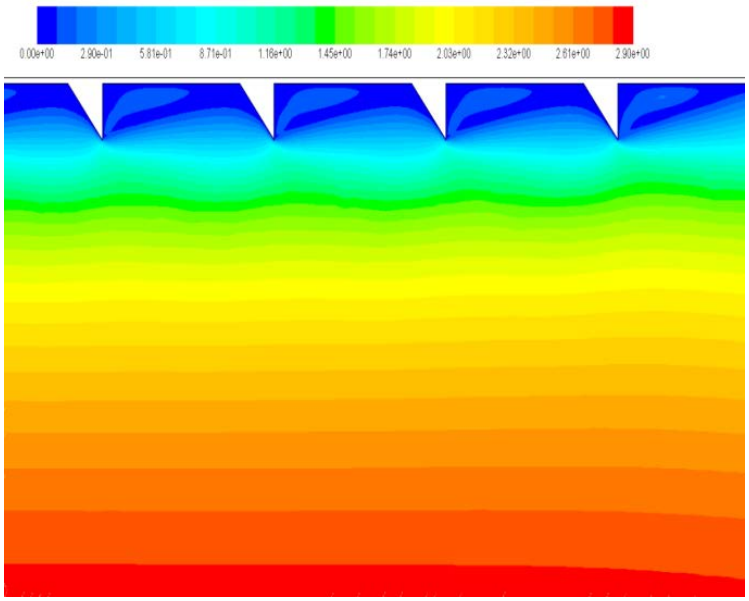

Fig. 7. Contour Plot for velocity magnitude for e=1.0 P=5 Re=5000.

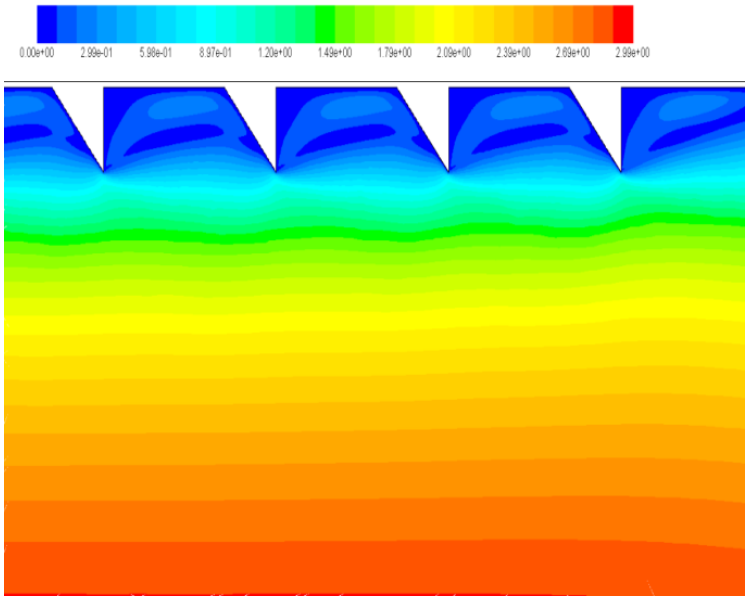

Fig. 8. Contour Plot for velocity magnitude for e=1.5 P=5 Re=5000.

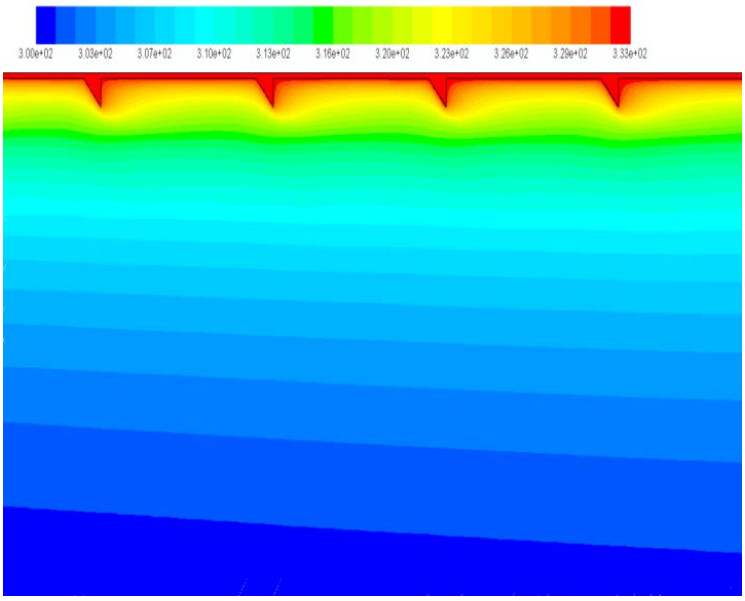

Fig. 9. Contour Plot for static temperature for e=0.5 P=5 Re=5000.

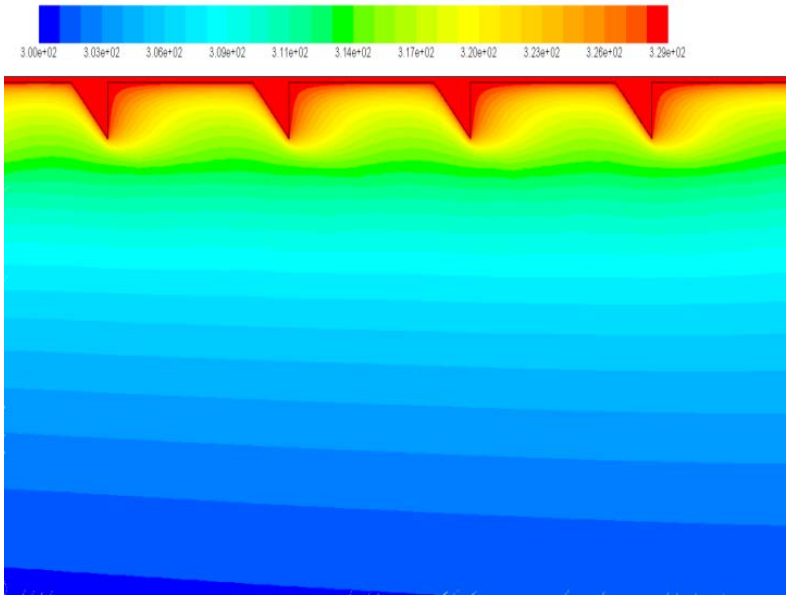

Fig. 10. Contour Plot for static temperature for e=1.0 P=5, Re=5000.

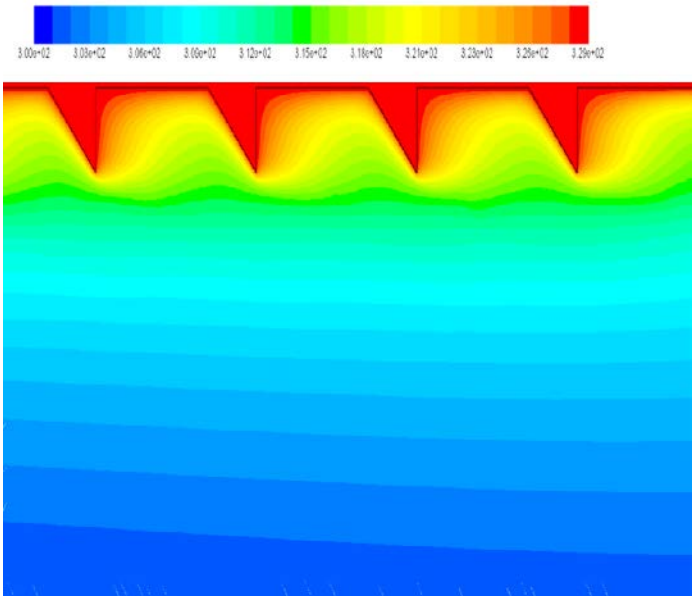

Fig. 11. Contour Plot for static temperature for e=1.5 P=5 Re=5000.

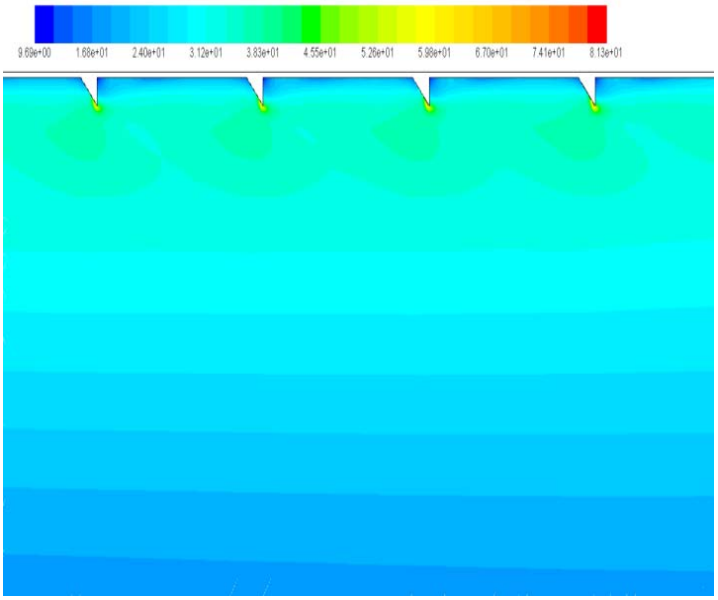

Fig. 12. Contour Plot for turbulence intensity for e=0.5 P=5 Re=5000.

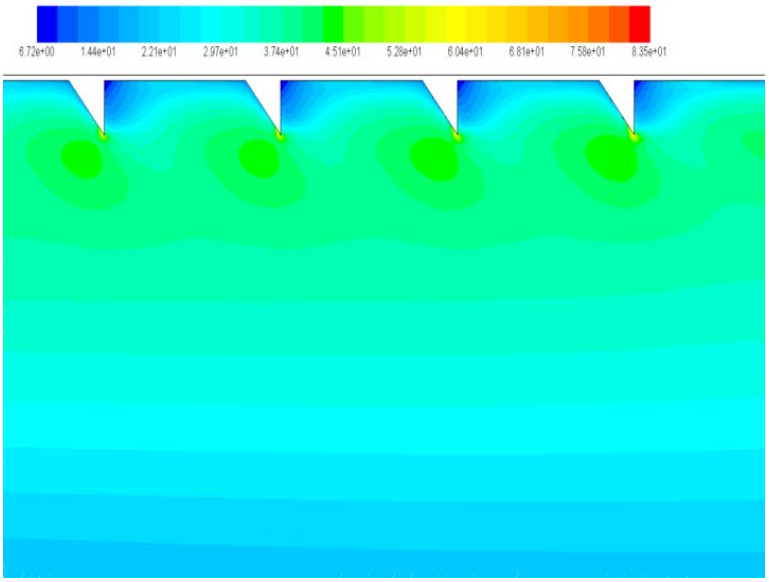

Fig. 13. Contour Plot for turbulence intensity for e=1.0 P=5 Re=5000.

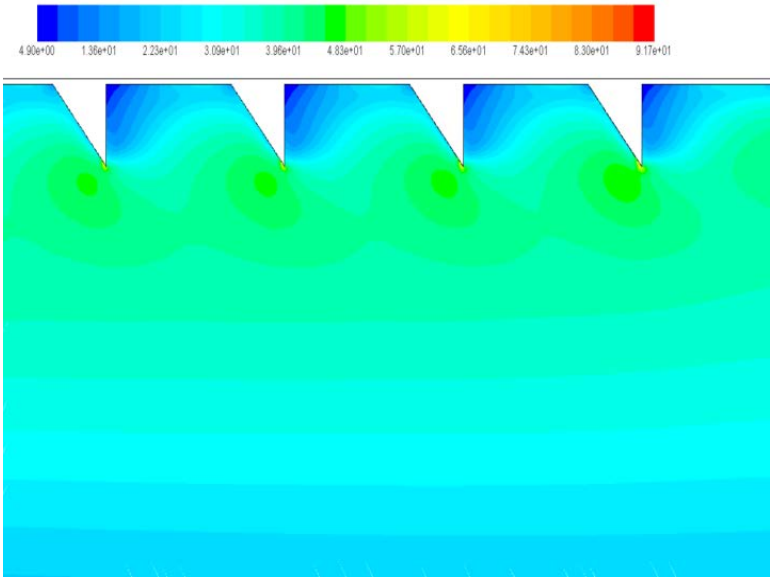

Fig. 14. Contour Plot for turbulence intensity for e=1.5 P=5 Re=5000.

3.2 Heat Transfer Results

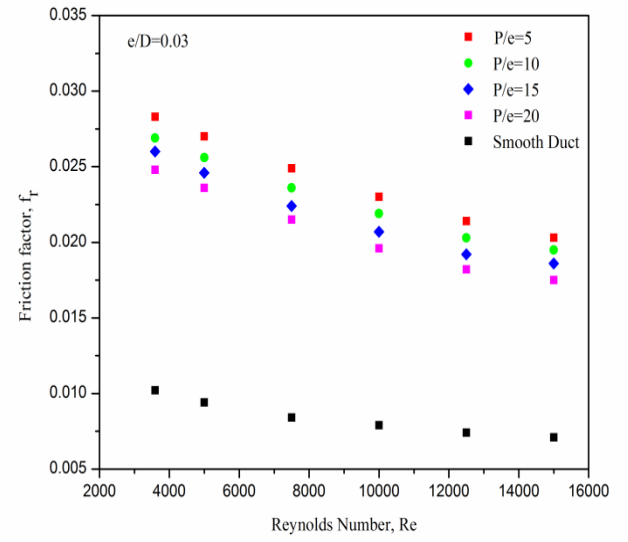

Fig.15. Variation of friction factor vs. Reynolds number at different P/e and fixed e/D.

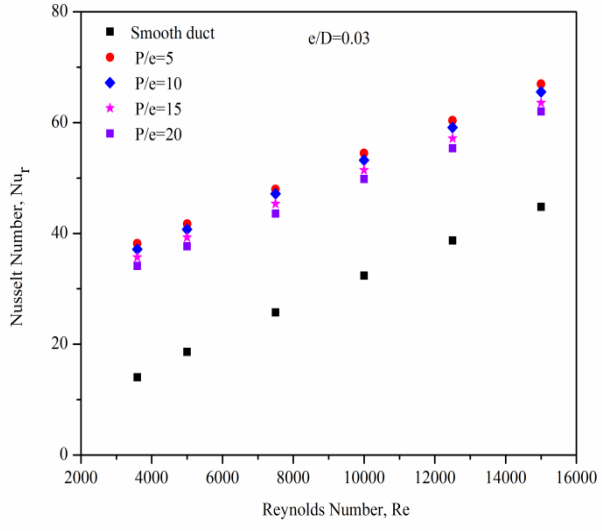

Fig.16. Variation of Nusselt number vs Reynolds number at different P/e and fixed e/D.

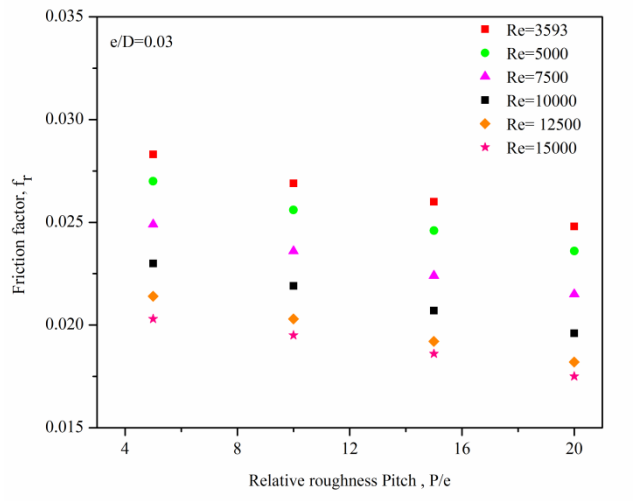

Fig. 17. Variation of friction factor vs. relative roughness pitch, P/e.

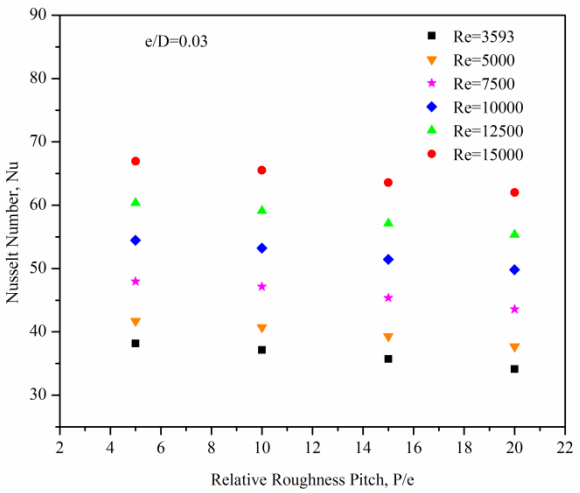

Fig. 18. Variation of Nusselt number vs. relative roughness pitch , P/e.

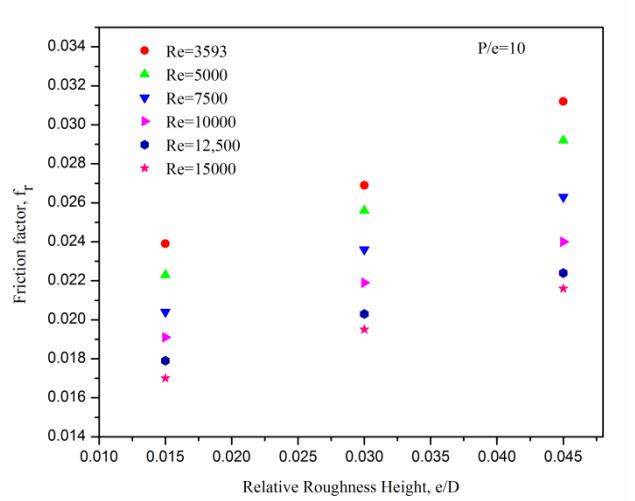

Fig. 19. -Friction factor as a function of relative roughness height for P/e=10.

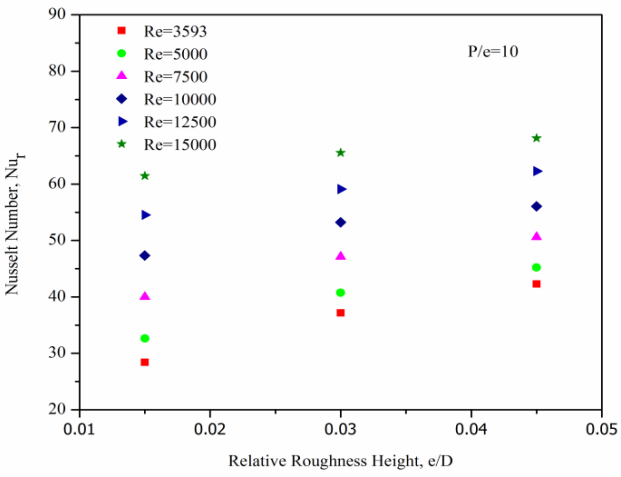

Fig. 20: Nusselt number as a function of relative roughness height for P/e=10.

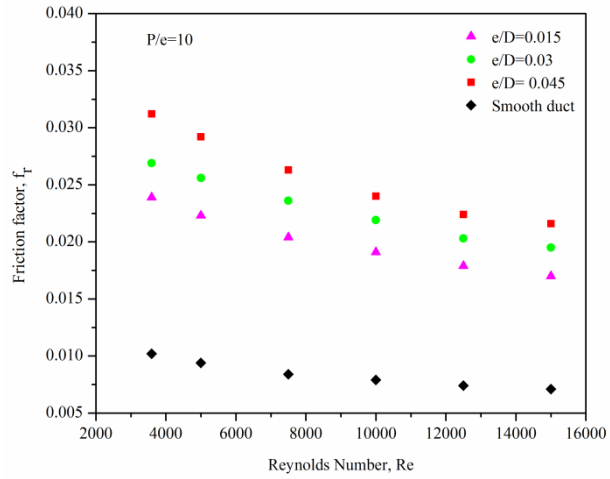

Fig. 21. Variation of friction factor with Reynolds number and for different values of e/D and fixed value of P/e.

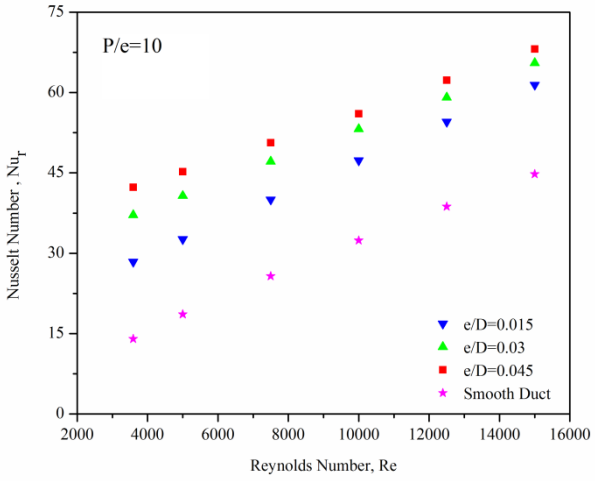

Fig. 22. Variation of Nusselt number with Reynolds number and for different values of e/D and fixed value of P/e.

3.3 Thermohydraulic Performance

Figure 22 shows the variation of thermo-hydraulic performance with the relative roughness pitch and Reynolds number at fixed value of relative roughness height. It is found that THPP values lies between 1.56 to 3.02. It is found that isosceles right triangle sectioned transverse rib roughness on the absorber plate with Pitch (P) =5mm and rib (e) =1mm gives better thermal performance.

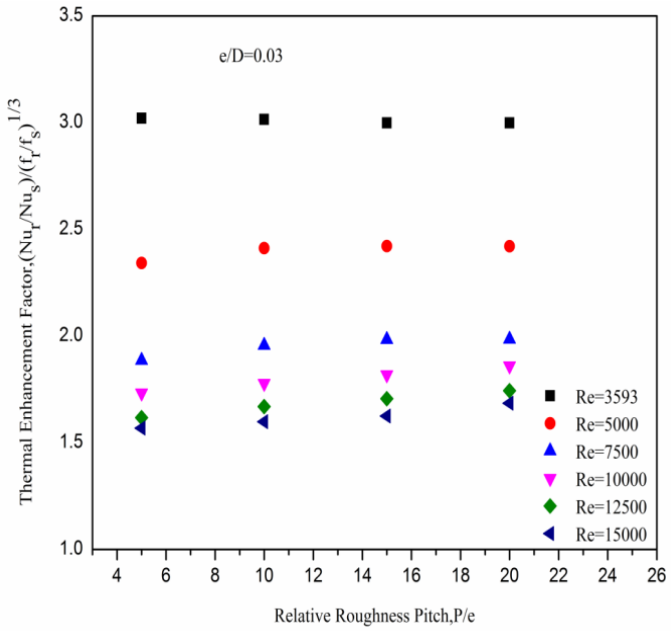

Fig. 23. Variation of thermo-hydraulic performance with the relative roughness pitch and Reynolds number at fixed value of Relative roughness height.

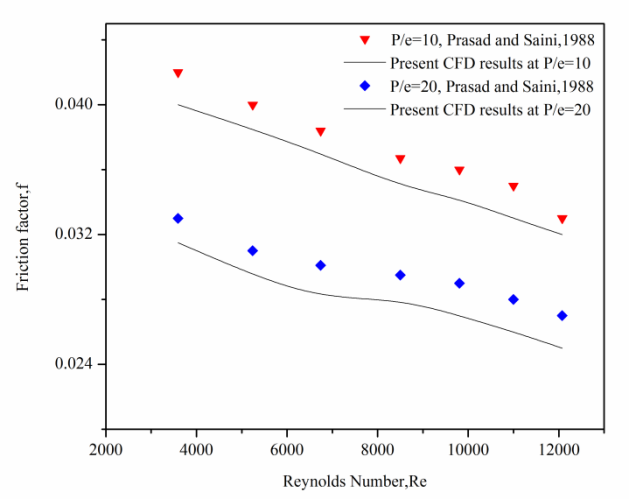

Fig. 24. Comparison of friction factor predicted by present CFD work with the previous experimental results of Prasad and Saini[28].

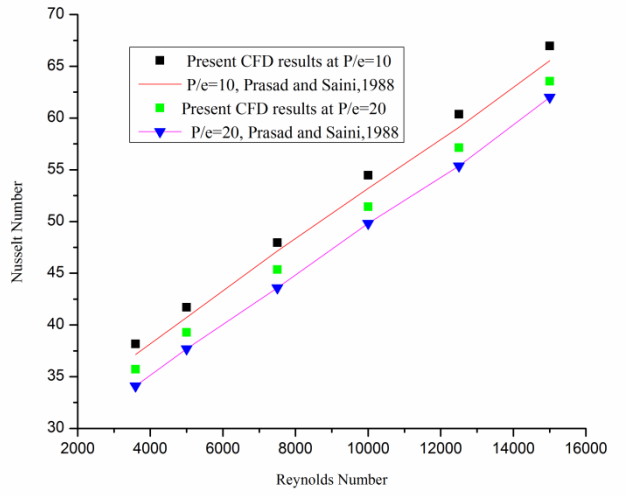

Fig. 25.Comparision of Nusselt number predicted by present CFD work with the previous experimental results of Prasad and Saini [28].

3.4 Validation of CFD Results

To validate the present numerical model, the results are compared with experimental results of different roughness geometries of similar trends for heat transfer and fluid friction for Prasad and Saini [28]. It can be seen that there show good agreement with experimental and CFD work. The discrepancy between the results Prasad and Saini and the CFD results is less than $\pm 10\%$. It has been observed that the proposed model of artificially roughened solar air heat predicts the experimental data quite accurately.

4. CORELATIONS FOR NUSSELT NUMBER AND FRICTION FACTOR

It has been seen that Nusselt number and friction factor are strong functions of the geometric and the flow parameters. Functional relationship for Nusselt number and friction factor written as:

$Nu_r = Nu\ (Re, P/e, e/D,)$ for α=45(fixed) (17)

and; $f_r = f\ (Re, P/e, e/D,)$ for α=45(fixed) (18)

5. CORRELATION FOR NUSSELT NUMBER

Figure 24 represents the CFD values of Nusselt number as a function of Reynolds number for the range of Parameters investigated at α=45° (fixed). Consequently the functional relationship between Nu and Re is written by utilizing the regression analysis to fit the straight line through the data points by Equation 19 as under:

$$Nu_r = A_0\,(Re)^{0.655} \quad (19)$$

Where A_0 is the function of parameters *i.e* relative roughness pitch (P/e) and relative roughness height (e/D).

Figure 25 is plotted P/e and $Nu_r/(Re)^{0.655}$ to yield Equation 20 as under

$$Nu_r = B_0\,(Re)^{0.655}(P/e)^{-0.143} \quad (20)$$

Where B_0 is the function of other influencing parameter, e/D.

Figure 27 is drawn to yield in Equation 21 as under for the heat transfer coefficient parameter, Nu_r:

$$Nu_r = C_0(Re)^{0.655}(P/e)^{-0.143}(e/D)^{0.312} \quad (21)$$

The value of C_0= 0.6312 when substituted in Equation 22 as under the heat transfer parameter Nu_r:

$$Nu_r = 0.6312(Re)^{0.655}(P/e)^{-0.143}(e/D)^{0.312} \quad (22)$$

Final correlation for Nusselt number:

$$Nu_r = 0.6312(Re)^{0.655}(P/e)^{-0.143}(e/D)^{0.312} \quad (23)$$

6. CORRELATION FOR FRICTION FACTOR

Similarly Figures 28 to 30 are drawn and correlation for friction factor are developed as Equation 24 written under:

$$f_r = 1.1621(Re)^{-0.1713}(P/e)^{-0.411}(e/D)^{0.321} \quad (24)$$

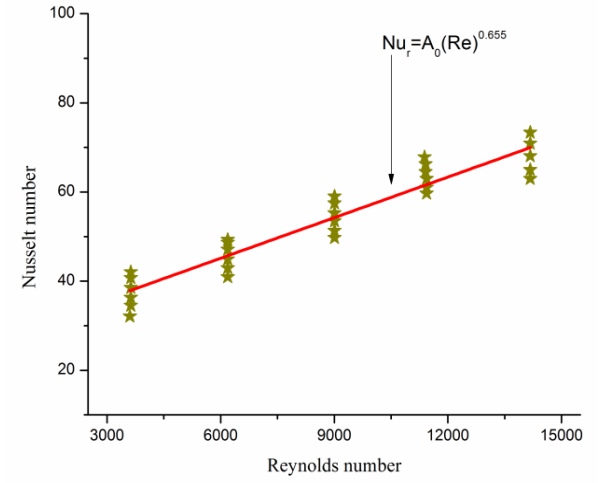

Fig. 26. Plot of Nu Vs. Re.

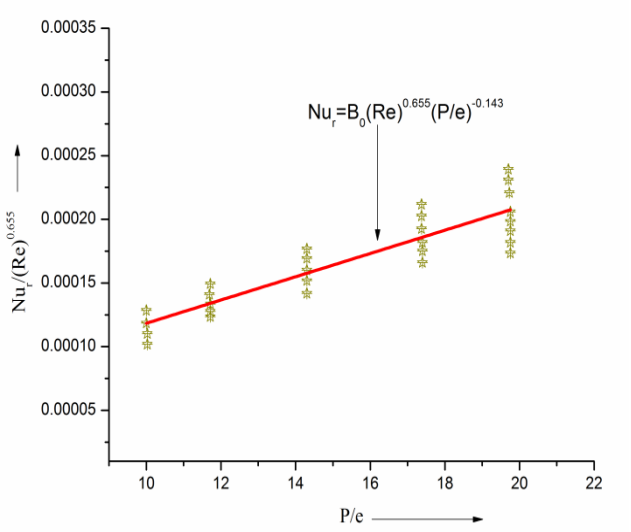

Fig. 27. Plot of $Nu_r/(Re)^{0.655}$ vs.P/e.

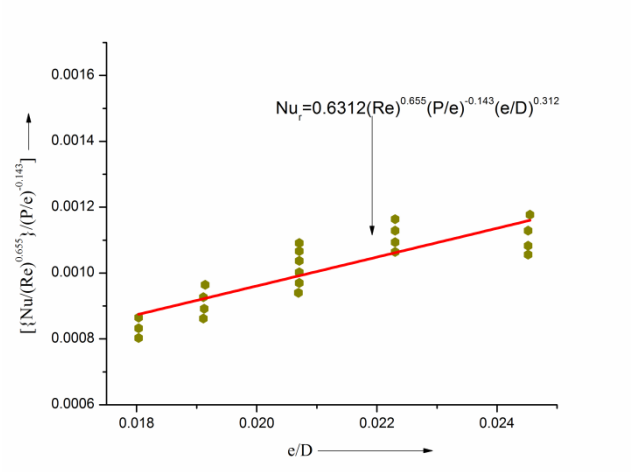

Fig. 28. Plot of [{Nu/(Re)$^{0.655}$}/(P/e)$^{-0.}$143] vs.e/D.

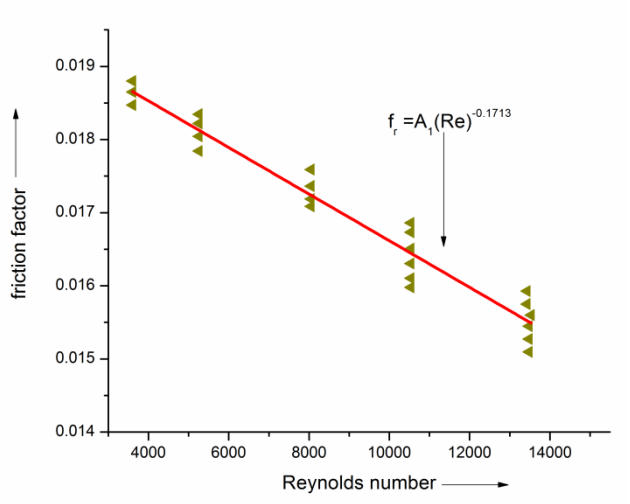

Fig. 29. Plot of f_r vs. Re.

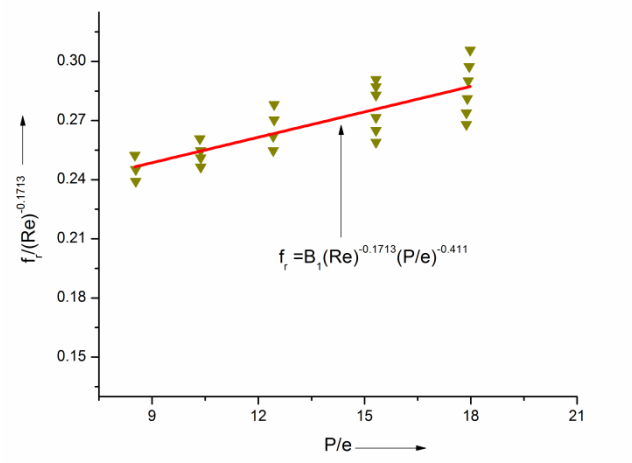

Fig. 30. Plot of $f_r/(Re)^{-0.1713}$vs. P/e.

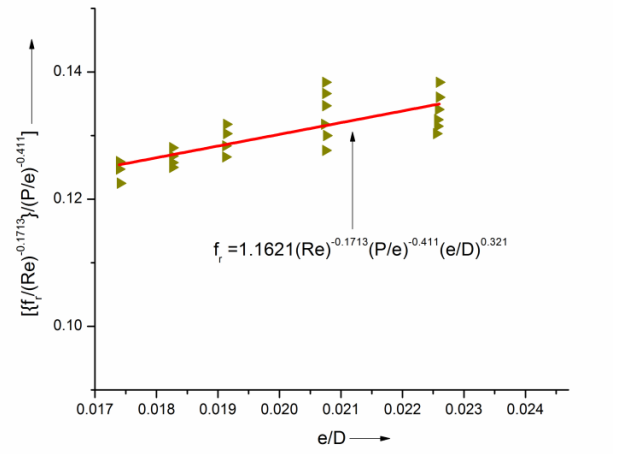

Fig. 31. [{$f_r/(Re)^{-0.1713}$}/$(P/e)^{-0.411}$] vs. e/D.

4. CONCLUSIONS

On the basis of the results and discuss the following conclusion has been drawn:

1. CFD has been applied in design of solar air heater. The quality of the solutions obtained from CFD simulations are largely within the acceptable range providing that CFD is an effective tool for predicting the behavior and performance of a solar air heater.
2. Nusselet number increases with the increase of Reynolds number .Solar air heater with isosceles right triangle gives 3.06 times enhancement in Nusselt number in comparison to that of a smooth plate.
3. Roughened absorber plates perform better at lower Reynolds number and smooth plates should be preferred when operating at higher Reynolds number. The maximum average Nusselt number is 70 for relative roughness pitch 3.33and relative roughness height 0.045.
4. Maximum thermo-hydraulic performance is obtained for relative roughness pitch of 5 and relative roughness height 0.03.
5. The maximum enhancement of friction factor 3.45 times in comparison over the smooth plate.
6. Statistical correlations for Nusselt number and friction factor have been developed. These correlations have been found to predict the value within the error limits

NOMENCLATURE

e	Roughness height, mm
l	Projected length of metal grit perpendicular to direction of flow, mm
s	Projected length of metal grit parallel to direction of flow, mm
k	Thermal conductivity of air, W/mk
f	Friction factor
P	Roughness pitch length, mm
D	Hydraulic diameter, mm
C_p	Specific heat of air, J/kg K
W	Width of duct, mm
H	Height of duct, mm
T	Temperature, K
K	Turbulence kinetic energy
L1	Entrance length, mm

L2 Test section length, mm
L3 Exit length, mm
I Turbulence intensity
Nu Nusselt number
Re Reynolds number
Pr Prandtl Number
St Stanton Number

SUBSCRIPTS

s Smooth
r Roughened
t Turbulent
a Ambient
i Inlet
o outlet
f Fluid

GREEK SYMBOLS

Φ Chamfer angle, deg
α Angle of attack, deg
θ Groove angle, deg
ΔP Pressure drop, pa
E Rate of dissipation
η Thermo-Hydraulic Performance

ACRONYMS

SIMPLE Semi-Implicit method for pressure linked equations
THPP Thermo-Hydraulic Performance Parameter

REFERENCES

[1] Joule J.P., 1861. On the surface condensation of steam. *Philosophical Transactions of the Royal Society of London*, 151:133-6.
[2] Nunner W., 1958. Heat transfer and pressure drop in rough pipes. *Vol. 22, VDI- Forsch, 1956, 445-B, English Trans, AERE Lib / Trans*, 786.
[3] Nikuradse J., 1950. Laws of flow in rough pipes. *NACA Technical Memorandum*, 1292.
[4] Dippery D.F. and R.H. Sabersky. 1963. Heat and momentum transfer in smooth and rough tubes at various Prandtl number. *International Journal of Heat and Mass Transfer* 6: 329-53.
[5] Prasad K. and S.C. Mullick. 1983. Heat transfer characteristics of a solar air heater used for drying purposes. *Applied Energy* 13(2): 83-93.
[6] Hans V.S., Saini R.P., and Saini J.S., 2009. Performance of artificially roughened solar air heaters- a review. *Renewable and Sustainable Energy Reviews* 13: 1854-69.
[7] Bhushan B and R. Singh. 2010. A review on methodology of artificial roughness used in duct of solar air heaters. *Energy* 35: 202-12.
[8] Kumar A., Saini R.P., and Saini J.S., 2012. Heat and fluid flow characteristics of roughened solar air heater ducts e a review. *Renewable Energy* 47:77-94.
[9] Karwa R., Solanki S.C., and Saini J.S., 2001. Thermo-hydraulic performance of solar air heaters having integral chamfered rib roughness on absorber plates. *Energy* 26: 161-76.
[10] Saini R.P. and J. Verma. 2008. Heat transfer and friction factor correlations for a duct having dimple-shaped artificial roughness for solar air heaters. *Energy* 33: 1277-87.
[11] Singh S., Chander S., and Saini J.S, 2011. Heat transfer and friction factor correlations of solar air heater ducts artificially roughened with discrete V-down ribs. *Energy* 36: 5053-64.
[12] Tanda G., 2011. Performance of solar air heater ducts with different types of ribs on the absorber plate. *Energy* 36: 6651-60.
[13] Lanjewar A., Bhagoria J.L., and Sarviya R.M., 2011. Heat transfer and friction in solar air heater duct with W-shaped rib roughness on absorber plate. *Energy* 36: 4531-41.
[14] Bhagoria J.L., Saini J.S., and Solanki S.C., 2002. Heat transfer coefficient and friction factor correlations for rectangular solar air heater duct having transverse wedge shaped rib roughness on the absorber plate. *Renewable Energy* 25: 341-69.
[15] Kumar A., Bhagoria J.L., and Sarviya R.M., 2009. Heat transfer and friction correlations for artificially roughened solar air heater duct with discrete W shaped ribs. *Energy Conversion and Management* 50: 2106-17.
[16] Yadav A.S. and J.L. Bhagoria. 2013. A CFD based heat transfer and fluid flow analysis of a solar air heater provided with circular transverse wire rib roughness on the absorber plate. *Energy* 55: 1127–1142.
[17] Yadav A.S. and J.L. Bhagoria. 2013. Modeling and simulation of turbulent flow through a solar air heater having a square-sectioned transverse rib roughness on absorber plate. *The Scientific World Journal*, http://dx.doi.org/10.1155/2013/827131.
[18] Chaube A., Sahoo P.K., and Solanki S.C., 2006. Analysis of heat transfer augmentation and flow characteristics due to rib roughness over absorber plate of a solar air heater. *Renewable Energy* 31: 317-331.
[19] Kumar S. and R.P. Saini. 2009. CFD based performance analysis of a solar air heater duct provided with artificial roughness. *Renewable Energy* 34: 1285-1291.
[20] Karmare S.V. and A.N. Tikekar. 2007. Heat transfer and friction factor correlation for artificially roughened ducts with metal grit ribs. *Int. J. Heat Mass Transfer* 50: 4342-4351.
[21] Hans V.S., Saini R.P., and Saini J.S., 2010. Heat transfer and friction factor correlations for a solar air heater duct roughened artificially with multiple v-ribs. *Solar Energy* 84:898-911.
[22] ASHRAE Standard 93-2003, 2003. Method of Testing to determine the Thermal Performance of Solar Collector.
[23] Launder B.E and D.B. Splading. 1972. *Lectures in Mathematical models of Turbulence*. Academic Press, London UK.

[24] Webb R.L. and E.R.G. Eckert. 1972. Application rough surfaces to heat exchanger design. *International Journal of Heat and Mass Transfer*, 15: 1647-1658.

[25] McAdams W.H., 1942. *Heat Transmission*, New York: McGraw-Hill.

[26] Fox W., Pritchard P., and McDonald A., 2010. *Introduction to Fluid Mechanics*, New York: John Wiley & Sons, pp. 754.

[27] ANSYS FLUENT. 14.5. Documentation. ANSYS, Inc; 2003-04.

[28] Prasad B.N. and J.S. Saini. 1988. Effect of artificial roughness on heat transfer and friction factor in a solar air heater. *Solar Energy* 41(6): 555–60.